Continuous Conduction Mode Soft-Switching Boost Converter and its Application in Power Factor Correction

Miao-miao Cheng [†], Zhiguo Liu [*], Yueyue Bao [*], and Zhongjie Zhang [*]

[†,*]College of Electrical and Information Engineering, Hunan University, Changsha, China

Abstract

Continuous conduction mode (CCM) boost converters are commonly used in home appliances and various industries because of their simple topology and low input current ripples. However, these converters suffer from several disadvantages, such as hard switching of the active switch and reverse recovery problems of the output diode. These disadvantages increase voltage stresses across the switch and output diode and thus contribute to switching losses and electromagnetic interference. A new topology is presented in this work to improve the switching characteristics of CCM boost converters. Zero-current turn-on and zero-voltage turn-off are achieved for the active switches. The reverse-recovery current is reduced by soft turning-off the output diode. In addition, an input current sensorless control is applied to the proposed topology by pre-calculating the duty cycles of the active switches. Power factor correction is thus achieved with less effort than that required in the traditional method. Simulation and experimental results verify the soft-switching characteristics of the proposed topology and the effectiveness of the proposed input current sensorless control.

Key words: Continuous conduction mode boost converter, Input current sensorless control, Power factor correction, Soft switching

I. INTRODUCTION

Pulse-width modulation (PWM) boost DC–DC converters are increasingly used in distributed generation systems, such as photovoltaic systems, fuel cell systems, and battery storage systems. In these applications, a boost converter can serve multiple functions by creating a higher regulating voltage. Boost converters are also the traditional method for implementing a front end with current regulation. The general requirements of boost converters are low reverse-recovery losses and low electromagnetic interference (EMI) problems. These requirements may be met by a soft-switching technique, which is a commonly used approach that switches under zero voltage or zero current and thus brings several advantages. For example, switching losses are eliminated, and voltage and current stress are reduced across the switches. A low di/dt or dv/dt also reduces EMI problems.

Recently, several soft-switching solutions have been proposed; these solutions employ auxiliary snubber cells or resonant converters and include quasi-resonant converters [1], active snubber [2], [3], asymmetrical half bridge [4], [5], and other schemes [6]-[8]. Among these topologies, a simple auxiliary resonant circuit, which includes an auxiliary switch, diode, resonant inductor, and resonant capacitor, is introduced to achieve zero-current turn-on and zero-voltage turn-off [9], [10]. A soft-switching converter with an edge-resonant capacitor module increases efficiency while achieving a high boost ratio [11]. Other topologies are also proposed to achieve zero-current turn-on and zero-current turn-off [12], [13].

The present work introduces the magnetic energy recovering switch (MERS) to achieve soft switching for the continuous conduction mode (CCM) boost converter. The MERS comprises a symmetric structure that simplifies control [14]. By turning the two switches on/off simultaneously, both zero-current turn-on and zero-voltage turn-off are achieved. Accordingly, the reverse-recovery problem of diodes is alleviated by smoothing the di/dt during
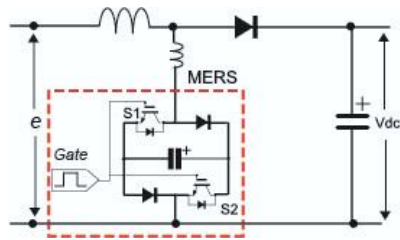
Fig. 1. Proposed soft-switching CCM boost converter.

current transition. As a typical application, the soft-switching boost converter is combined with a rectifier bridge to form a traditional power factor correction (PFC) circuit. PFC is essential for power supplies to comply with harmonics standards or recommendations [15]-[17]. Although bridgeless configurations are reportedly highly efficient, the boost converter-based PFC remains the most popular topology because of its simple scheme and low EMI [18], [19]. Furthermore, interleaved topologies with soft-switching characteristics have attracted attention in recent years [20]-[22], along with the interest in developing simple control strategies with good performance [23]-[25].

In this work, we first describe the operation principles for the MERS-based CCM boost converter. Soft-switching characteristics are illustrated, and a mathematical model is established for the proposed topology. Applications in PFC are then discussed. A current sensorless control is proposed for the soft-switching PFC boost converter. Unlike the traditional average current mode control, this control asks for no input current detection. Instead, boost switches are instructed by a pre-calculated duty cycle, which is synchronized with the AC voltage phase. Duty cycle calculations and analysis are explained in detail. Finally, simulation and experiments are performed to verify the proposed soft-switching topology and the current sensorless PFC control.

II. OPERATION PRINCIPLES OF THE PROPOSED SOFT-SWITCHING BOOST CONVERTER

The configuration of the proposed soft-switching boost converter is shown in Fig. 1. The main switch in the traditional converter is replaced in the proposed converter with a magnetic energy recovering switch (MERS). The MERS consists of two forced commutated switches, two diodes, and a DC capacitor. The charging/discharging of the DC capacitor achieves zero-voltage turn-off for the active switches. A small inductor is inserted to the MERS branch to achieve the zero-current turn-on of the active switches and the soft turn-off of the output diode even at CCM operation.

A. Operation States

The operation states of the proposed configuration and the soft-switching principles are illustrated in Fig. 2. For every switching cycle, the MERS capacitor charges to near-output
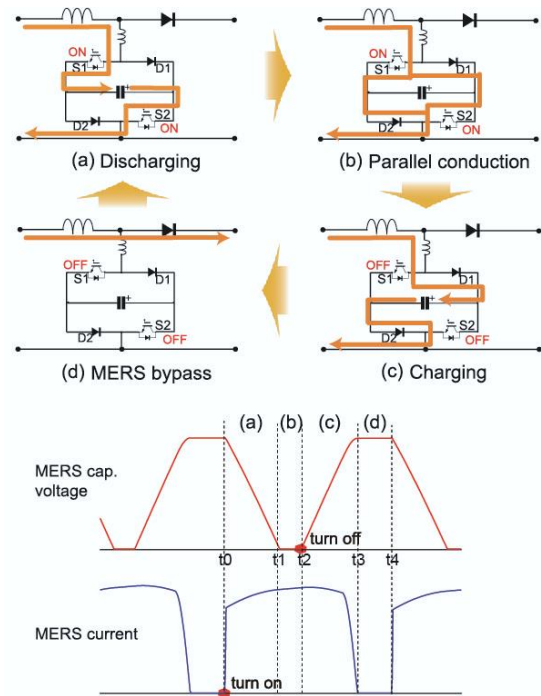

Fig. 2. Operation states and soft-switching principles of the proposed CCM boost converter.

voltage and discharges to zero. The active switches achieve zero-voltage turn-off within this zero-voltage period. Zero-voltage turn-on is also achieved for the output diode because of the charging of the MERS capacitor. An entire switching cycle includes the following four operation states.

1) Discharging. The MERS capacitor discharges once the active switches are turned on. The current flowing through the output diode shifts to the MERS branch. The inductor inserted in the MERS branch ensures the zero-current turn-on of the active switches. The soft turn-off of the output diode is also achieved with a reduced current change velocity.

2) Parallel conduction. Once the MERS capacitor voltage discharges to zero, the operation shifts to the parallel conduction state. The MERS current splits into two paths, and each switch shares half the MERS current. This state ends once the active switches are turned off. At this point, zero-voltage turn-off is realized for the active switches.

3) Charging. The input current charges the MERS capacitor when the active switches are turned off. Once the MERS branch voltage reaches the output voltage, the output diode conducts, and zero-voltage turn-on is achieved for the output diode. As a result of the inductance inserted in the MERS branch, the input current shifts gradually from the MERS branch to the output diode. The current change velocity of the output diode is reduced.

4) MERS bypass. The MERS branch is bypassed until the active switches are turned on.

B. Mathematical Model

Two assumptions are established to simplify the mathematical descriptions. First, the output capacitance is large enough to regulate the output voltage to a stable value, which is V_{dc} in Fig. 1. Second, the inductance inserted into the MERS branch is negligible because its value is much smaller than the input inductance. Finally, the following voltage/current equations are obtained to describe the four operation modes in a switching cycle.

In discharging state (a), we have

$$LC\frac{d^2 u_C}{dt^2} + u_C + e = 0 \tag{1}$$

with the conditions $u_{C(t=t0)} = V_{dc}$ and $-C\frac{du_c}{dt}\Big|_{(t=t0)} = i_{L(t0)}$. L and C are the input inductance and capacitance of the MERS capacitor, respectively; u_C and e are the instantaneous MERS capacitor voltage and input voltage, respectively; and $i_{L(t0)}$ is the initial inductor current at the beginning of state (a). By solving this equation, we obtain

$$\begin{cases} u_{C(t)} = (V_{dc}+e)\cos\frac{t-t0}{\sqrt{LC}} - i_{L(t0)}\sqrt{\frac{L}{C}}\sin\frac{t-t0}{\sqrt{LC}} - e \tag{2} \\[4mm] i_{L(t)} = \sqrt{\frac{C}{L}}(V_{dc}+e)\sin\frac{t-t0}{\sqrt{LC}} + i_{L(t0)}\cos\frac{t-t0}{\sqrt{LC}} \tag{3} \end{cases}$$

with the condition $t \in [t0, t1]$.
In parallel conduction state (b), we obtain

$$\begin{cases} u_{C(t)} = 0 \tag{4} \\[4mm] i_{L(t)} = i_{L(t1)} + \frac{e}{L}(t-t1) \tag{5} \end{cases}$$

with the condition $t \in [t1, t2]$.

In charging state (c), we have

$$LC\frac{d^2 u_C}{dt^2} + u_C - e = 0 \tag{6}$$

with the conditions $u_{C(t=t2)} = 0$ and $C\frac{du_c}{dt}\Big|_{(t=t2)} = i_{L(t2)}$.

By solving this equation, we obtain

$$\begin{cases} u_{C(t)} = -e\cos\frac{t-t2}{\sqrt{LC}} + i_{L(t2)}\sqrt{\frac{L}{C}}\sin\frac{t-t2}{\sqrt{LC}} + e \tag{7} \\[4mm] i_{L(t)} = \sqrt{\frac{C}{L}}e\sin\frac{t-t2}{\sqrt{LC}} + i_{L(t2)}\cos\frac{t-t2}{\sqrt{LC}} \tag{8} \end{cases}$$

with the condition $t \in [t2, t3]$.
In MERS bypass state (d), we obtain

$$\begin{cases} u_{C(t)} = V_{dc} \tag{9} \\[4mm] i_{L(t)} = i_{L(t3)} + \frac{e-V_{dc}}{L}(t-t3) \tag{10} \end{cases}$$

with the condition $t \in [t3, t4]$.

On basis of the above equations, the MERS capacitor voltage curve and input inductor current curve are determined with the given input/output voltage and fixed circuit parameters.
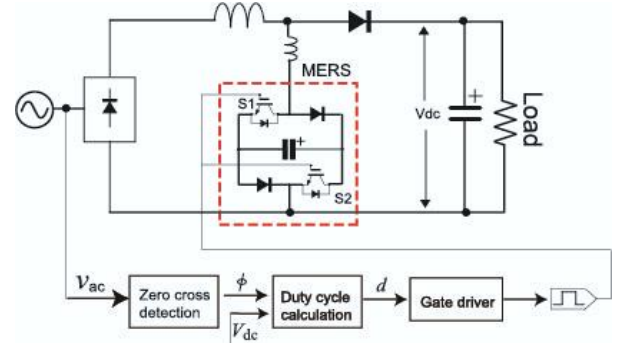

Fig. 3. Proposed soft-switching CCM-PFC converter.

III. APPLYING THE PROPOSED SOFT-SWITCHING BOOST TOPOLOGY FOR THE CCM-PFC CONVERTER

The proposed soft-switching boost topology is combined with a rectifier bridge to form a CCM-PFC circuit, as shown in Fig. 3. Traditionally, the instantaneous input current is detected and regulated to follow the phase of the input voltage. As the instantaneous current detection requires much effort to implement, a current sensorless control is proposed. In this control, the desired duty cycle for the active switches of the MERS is first calculated offline on the basis of the established mathematical model. The CCM PFC is then achieved by driving the active switches with the calculated duty cycle.

A. Calculation for the Desired Duty Cycle

The active switches of the MERS are turned on and off simultaneously. Using the mathematical model established in the last section, the expected duty cycle of the active switches is pre-calculated in this part. The rectifier voltage e is assumed to be constant within one switching cycle considering that the switching frequency is much higher than the line frequency. The process for calculating the desired duty cycle is described as follows.

First, inductor current i_L should trace the desired sine wave, which is in phase with rectifier voltage e. They are described as

$$e_{t0} = \left|\sqrt{2}V_{ac}\sin\omega t_0\right| \tag{11}$$

$$i_{L(t0)} = \left|\sqrt{2}I_{ac}\sin\omega t_0\right| \tag{12}$$

where e_{t0} and $i_{L(t0)}$ represent the rectifier voltage and inductor current at the beginning of a switching cycle, respectively.

Second, the instantaneous inductor current within the same switching cycle can be derived from the established mathematical model. For simplicity, the points of the inductor current, $i_{L(t1)}$, $i_{L(t2)}$, $i_{L(t3)}$, and $i_{L(t4)}$, are calculated with Eqs. 3, 5, 8, and 10. Particularly, we obtain $i_{L(t4)}$, which is described as a function of the duty cycle.

$$i_{L(t4)} = function(d) \tag{13}$$

Here, *d* represents the duty for this switching cycle.

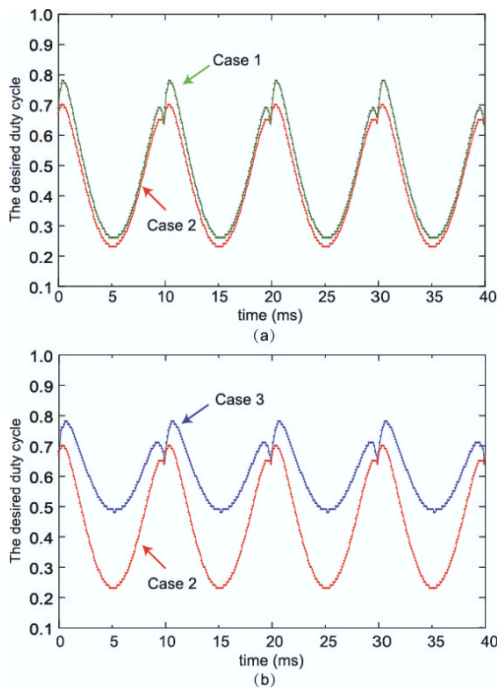| Variables	Case 1			Case 2			Case 3		
AC voltage, RMS, V_{ac}	50 V	100 V	200 V	50 V	100 V	200 V	50 V	100 V	200 V
DC voltage, V_{dc}	100 V	200 V	400 V	100 V	200 V	400 V	150 V	300 V	600 V
Resistive, R	50 Ω			100 Ω			100 Ω		
Input inductance, L	2.5 mH			2.5 mH			2.5 mH		
MERS capacitor, C	0.2 uF			0.2 uF			0.2 uF		
Switching frequency, f_{sw}	10k			10k			10k		

Fig. 4. Desired duty cycle results: (a) with a constant value of V_{dc}/V_{ac} and (b) with a constant value of load resistance, R.

Fig. 5. Simulation results of AC input voltage/current.

Third, $i_{L(t4)}$, which is also equal to the inductor current at the beginning of the next switching cycle, $i_{L(t0,next)}$, is assumed to have traced the desired sine wave and should be described as

$$i_{L(t0,next)} = \left| \sqrt{2} I_{ac} sin\omega(t_0 + T_{sw}) \right| \tag{14}$$

where T_{sw} is the switching cycle.

Finally, the desired duty cycle within this switching cycle is obtained by combining Eqs. 13 and 14.

B. Discussion of the Desired Duty Cycle Results

Calculations are performed to identify the desired duty results within a fundamental cycle. The calculation conditions are listed in Table I. The parameters of components L and C are constant for each group of data. The input/output voltage and load resistance are varied for comparison purposes. As shown in Table I, the boost ratios of the data groups of Cases 1 and 2 are the same, whereas their load resistances are different. Moreover, the load resistances of the data groups of Cases 2 and 3 are the same, whereas their boost ratios are
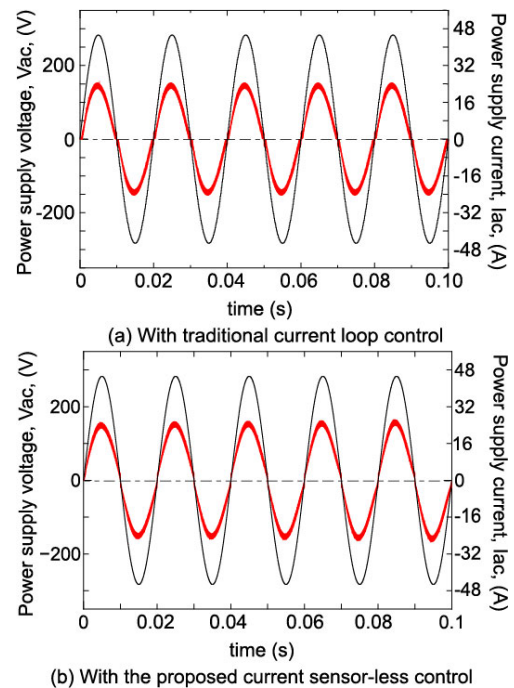
different.

The calculation results of the desired duty cycle (Fig. 4) reveal that the duty cycle is determined by two factors: the boost ratio and the load resistance. The desired duty cycle increases with the boost ratio, particularly in the valley area of the curve (Fig. 4(b)). Fig. 4(a) shows that load resistance affects the desired duty cycle as well. As load resistance increases, the desired duty decreases slightly. Every duty cycle curve shows a periodic change and is synchronized with the rectifier voltage. Therefore, instead of current detection, PFC could be realized by sensing the input voltage. As voltage detection is more convenient than instantaneous current detection, the required implementation effort is greatly reduced.

Finally, an input current sensorless control is proposed for PFC. The control diagram is depicted in Fig. 3. The phase of the input voltage is sensed and provided for the duty cycle calculation. The desired duty cycle then instructs the gate driver for the MERSs. The duty cycle calculation can also be performed offline, thus simplifying control.
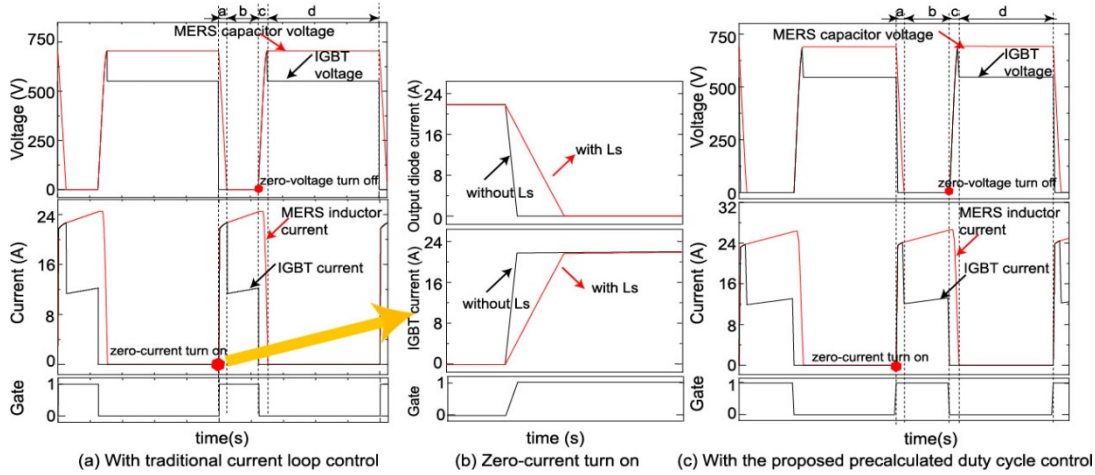
Fig. 6. Verifications for the soft-switching of the proposed topology: zero-voltage turn off and zero-current turn on.
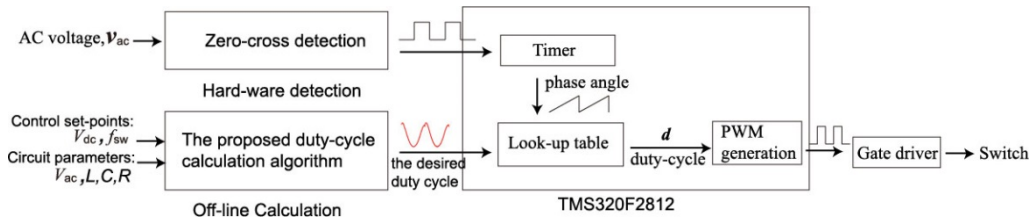

Fig. 7. Utilized control circuit diagram.

IV. SIMULATION VERIFICATIONS FOR THE PROPOSED CCM-PFC

Simulations are performed using the proposed topology with the proposed input current sensorless control. The proposed topology is verified with soft-switching characteristics at CCM operation. Then, the input current sensorless control is verified to realize PFC.

A. Using Traditional Current Loop Control

A traditional current control loop is tested first for comparison purposes. The input current is sensed and forced to track the phase of the AC voltage. The simulation circuit parameters are given in Table I. A small inductor (40 *u*H) is inserted to the MERS branch to achieve zero-current turn-on for the active switches. The RMS values of the AC voltage, DC voltage, and load resistance are 200 V, 400 V, and 50 Ω, respectively, and are the same as those of group 3 of Case 1.

The simulation results are given in Figs. 5 and 6. The input current is continuous and in phase with the AC voltage (Fig. 5(a)). The power factor reaches as high as 0.996. The THD of the input current is approximately 0.06. Fig. 6(a) shows the switch voltage and current during a switching cycle. Both zero-voltage turn-off and zero-current turn-on are achieved for the switches. As a result of the insertion of the inductor into the MERS branch, the di/dt is greatly decreased during the transition of the current from the output diode to the MERS branch (Fig. 6(b)). The reverse-recovery problem is alleviated for the output diode. These results prove that the proposed topology features soft-switching characteristics

when operating as a CCM-PFC converter.

B. Using proposed input current sensorless control

Simulations with the same conditions are conducted with the proposed input current sensorless control. No current is detected, and the desired duty cycle is pre-calculated using the established mathematical model. The simulation results are shown in Figs. 5(b) and 6(c).

Fig. 5(b) shows the AC input current and input voltage. The input power factor is approximately 0.996, and the THD of the input current is approximately 0.06; both values are in good agreement with those in Fig. 5(a). The MERSs achieve soft switching in the simulation results shown in Fig. 6(c) and are in good accordance with the results in Fig. 6(a). This outcome proves the effectiveness of the proposed input current sensorless control for CCM-PFC converters. The proposed configuration shows good soft-switching characteristics as well.

V. EXPERIMENTAL VERIFICATION OF THE PROPOSED CCM-PFC

Experiments are conducted to verify the proposed configuration and input current sensorless control. Two aspects are highlighted: the input power factor should be regulated by the sensorless current control, and the soft-switching characteristics are inherent to the proposed topology.

A. Experimental Procedure

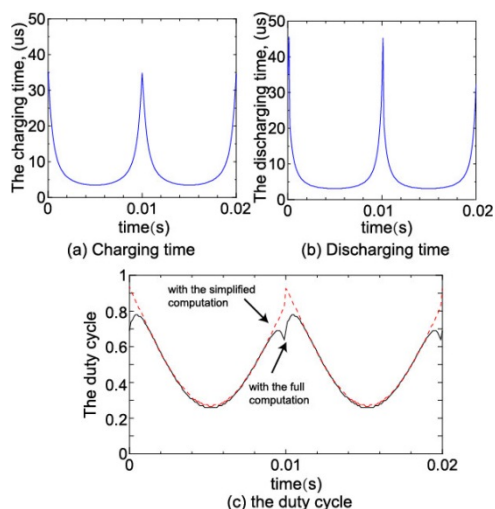| Variables	Case 1	Case 2
AC voltage, RMS, V_{ac}	50 V	100 V
DC voltage, V_{dc}	100 V	200 V
Resistive, R	50 Ω	100 Ω
Input inductance, L	2.5 mH	2.5 mH
MERS capacitor, C	0.2 μF	0.2 μF
Switching frequency, f_{sw}	10k	10k

Fig. 8. Calculation results. (a) Charging time. (b) Discharging time. (c) The desired duty cycle.

The experimental conditions are listed in Table II. The circuit parameters are identical to those in the simulations. The utilized control circuit (Fig. 7) is composed of three parts. First, zero-cross detection detects the zero-cross point by transforming the input AC voltage into a rectangular wave. Second, duty cycle calculation is performed offline in MATLAB to obtain the desired duty cycle results for one whole fundamental cycle. Then, the rectangular wave signal of the zero-cross detection is used to generate the phase angle of AC voltage via a timer control. Third, the phase angle of the AC voltage and the desired duty cycle results are used to form a look-up table, which is embedded in a DSP controller. The DSP generates the gate signal to drive the active switches of the proposed circuit.

The core of the control is to calculate the desired duty cycle. This calculation is performed offline using the established mathematical model and the corresponding algorithm. Efforts are also exerted to further simplify the computation. The charging time ($T_{cha} = t_1 - t_0$) and discharging time ($T_{dis} = t_3 - t_2$) account for a large part of the entire computation. However, the results of charging and discharging time present a "U"-type wave in each fundamental cycle, as shown in Figs. 8(a) and (b). They demonstrate charging and discharging time results under the experimental conditions of Case 1. These two variables are
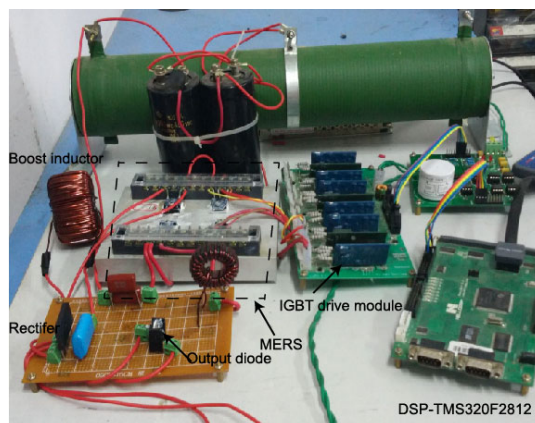

Fig. 9. Photograph of the experimental device.

assumed to have fixed values. The flat parts of the "U"-type wave are adopted for charging and discharging time. The corresponding duty cycle results in each fundamental frequency cycle are shown in Fig. 8(c). The red dotted curve denotes the simplified computation case, and the black solid curve represents the full computation case. The results of the desired duty cycles in a fundamental frequency cycle are almost similar.

B. Experimental Results

A photograph of the experimental device is shown in Fig. 9. The voltage and current of every part are detected using HIOKIMR8875. The experimental results from operating the MERSs with the desired duty cycles are shown in Figs. 10 and 11. Fig. 10 shows the experimental results of MERS voltage, IGBT voltage, MERS current, and IGBT current. Zero-voltage turn-off and zero-current turn-on are achieved for the active switches. The proposed configuration achieves soft-switching characteristics. Fig. 11 shows the experimental results of the input voltage and input current. The input current is almost in phase with the input voltage, thus proving that the proposed input current sensorless control achieves PFC with continuous input current.

C. Loss Considerations

As described previously, switching losses may be eliminated via the soft-switching operation. However, conduction losses may increase because of the number of switches in a current path. The converter efficiency should be studied to evaluate the proposed converter. Switch loss is calculated to compare the proposed topology with the traditional boost PFC converter. The circuit parameters are the same as those of group 3 of Case 1 (Table I). The RMS values of AC voltage, DC voltage, and load resistance are 200 V, 400 V, and 50 Ω, respectively. The calculations are performed on the basis of the datasheet of IGBT (FGA25N120ANTD) and DIODE (RHRP30120). The calculations of switch losses are listed in Table III. The loss produced by the MERS boost circuit is 39.94 W, whereas that
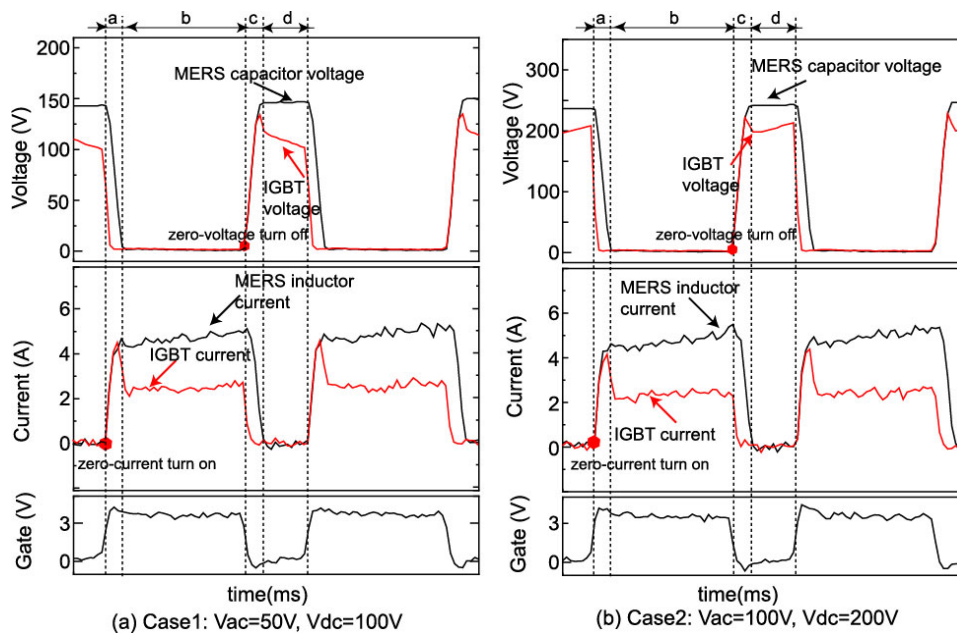
Fig. 10. Experimental verifications for the soft-switching of the proposed topology.

TABLE III
COMPARISON OF THE SWITCH LOSSES OF THE PROPOSED CIRCUIT AND TRADITIONAL CIRCUIT

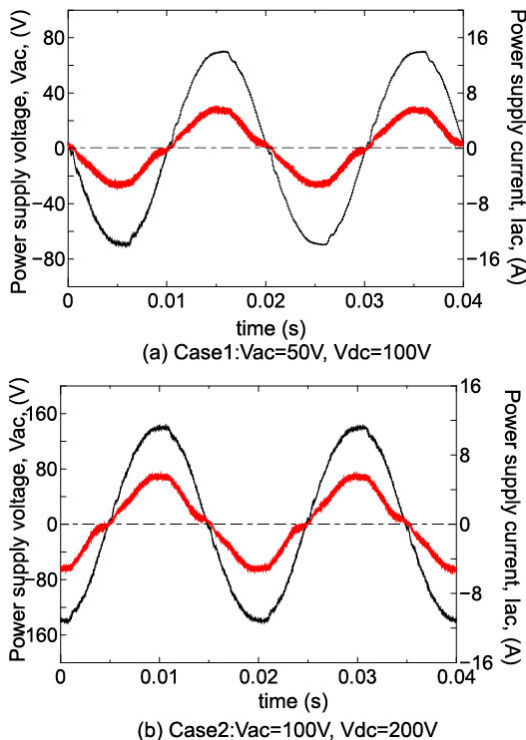|	Proposed circuit		Traditional circuit	
MERS	IGBT	6.21*2 W	Conduction loss	11.52 W
/boost switch	DIODE	5.75*2 W	on/off loss	29+10 W
Output diode	16.02 W		23.68 W	
Sum of switch losses	39.94 W		74.2 W	

Fig. 11. Experimental results of input voltage/current.

produced by the traditional boost circuit is 74.2 W. This result shows that the switch loss is approximately 46% lower in the soft-switching operation.

VI. CONCLUSIONS

CCM-PFC is the preferred technology to achieve a high power factor and low harmonic distortion, particularly at medium and high power levels. However, hard switching, reverse-recovery problems, and EMI are severe deficiencies. Furthermore, the requisite instantaneous current detection requires excessive implementation effort. To solve these issues, we propose a new soft-switching CCM-PFC topology and an input current sensorless control. The following conclusions are obtained.

1) A new boost converter is introduced to achieve zero-voltage turn-off and zero-current turn-on for the active switches even during CCM operation. The reverse-recovery problem is alleviated by soft turning-off the output diode.

2) A mathematical model of the proposed CCM-boost converter is established. By applying it with the PFC principle, an input current sensorless control method is developed. This new method is implemented by

operating the switches with pre-calculated duty cycles. PFC is thus achieved by simply sensing the phase of the input voltage. Moreover, the implementation effort is greatly reduced.

Simulations and experiments are performed using the new topology with the proposed input current sensorless control. The proposed CCM soft-switching boost converter and its application in PFC technology are proved to be effective and practical.

REFERENCES

[1] S. Sharifi and M. Jabbari, "Family of single-switch quasi-resonant converters with reduced inductor size," *IET Power Electron.*, Vol. 7, No. 10, pp. 2544-2554, Oct. 2014.

[2] H. Bodur and A. F. Bakan, "A new ZVT-ZCT-PWM DC-DC converter," *IEEE Trans. Power Electron.*, Vol. 19, No. 3, pp. 676-684, May 2004.

[3] R. L. Lin, Y. Zhao, and F. C. Lee, "Improved soft-switching ZVT converters with active snubber," *Applied Power Electronics Conference and Exposition (APEC)*, pp.1063- 1069, 1998.

[4] J. C. Huang, and W. L. Li, "A high-efficiency soft-switched AC/DC converter with current-doubler synchronous rectification," *IEEE Trans. Ind. Electron.*, Vol. 52, No. 3, pp. 709-718, May 2005.

[5] J. H. Liang, P. C. Wang, K. C. Huang, C. L. Chen, Y. H. Leu, and T.M. Chen, "Design optimization for asymmetrical half-bridge converters," *Applied Power Electronics Conference and Exposition (APEC)*, pp. 697-702, 2001.

[6] S. Park, and S. Choi, "Soft-switched CCM boost converter with high voltage gain for high power applications," *IEEE Trans. Power Electron.*, Vol. 25, No. 5, pp. 1211-1217, May 2010.

[7] W. H. Li, W. C. Li, Y. Deng, and X. N. He, "Single-stage single-phase high-step-up ZVT boost converter for fuel-cell microgrid system," *IEEE Trans. Power Electron.*, Vol. 25, No. 12, pp. 3057-3065, Dec.2010.

[8] H. L. Do, "A soft-switching DC/DC converter with high voltage gain," *IEEE Trans. Power Electron.*, Vol. 25, No. 5, pp. 1193-1200, May 2010.

[9] S. H. Park, G. R. Cha, Y. C. Jung, and C. Y. Won, "Design and application for PV generation system using a soft-switching boost converter With SARC," *IEEE Trans. Ind. Electron.*, Vol. 57, No. 2, pp. 515-522, Jan. 2010.

[10] D. Y. Jung, Y. H. Ji, S. H. Park, Y. C. Jung, and C. Y. Won, "Interleaved soft-switching boost converter for photovoltaic power generation system," *IEEE Trans. Power Electron.*, Vol. 26, No. 4, pp. 1137-1145, Jul.2011.

[11] T. Mishima,Y. Takeuchi, and M. Nakaoka, " A new high step-up voltage ratio soft switching PWM boost DC-DC power converter with edge resonant switched capacitor modular," *14th European Conference on Power Electronics and Applications (EPE)*, pp. 1-10, 2011.

[12] E. C. Dias, L. C. G. Freitas, E. A. A. Coelho, J. B. Vieira, and L. C. de Freitas, "Novel true zero current turn-on and turn-off converter family: analysis and experimental results," *IET Power Electron.*, Vol. 3, No. 1, pp. 33-42, Jan. 2010.

[13] P. Das, and G. Moschopoulos, "A comparative study of zero-current-transition PWM converters', *IEEE Trans. Ind. Electron.*, Vol. 54, No. 3,pp. 1319-1328, Apr. 2007.

[14] T. Isobe, Y. Miyaji, T. Kitahara, K. Fukutani, and R. Shimada, "Soft-switching inverter for variable frequency induction heating using magnetic energy recovery switch (MERS)," *13th European Conferenceon PowerElectronics and Applications (EPE)*, pp. 1-10, 2009.

[15] P. Das, M. Pahlevaninezhad, J. Drobnik, G. Moschopoulos, and P. K. Jain, "A nonlinear controller based on a discrete energy function for an AC/DC boost PFC converter," *IEEE Trans. Power Electron.*, Vol. 28, No. 12, pp. 5458-5476, Dec. 2013.

[16] Y. S. Kim, W. Y. Sung, and B. K. Lee, "Comparative performance analysis of high density and efficiency PFC topologies," *IEEE Trans. Power Electron.*, Vol. 29, No. 6, pp. 2666-2679, Jun. 2014.

[17] L. Huber, Y. Jang, and M. M. Jovanovic, "Performance evaluation of bridgeless PFC boost rectifiers," *IEEE Trans. Power Electron.*, Vol. 23, No. 3, pp. 1381-1390, May 2008.

[18] Z. Ye, and B.S Sun, "PFC efficiency improvement and THD reduction at light loads with ZVS and valley switching," *Applied Power Electronics Conference and Exposition (APEC)*, pp. 802-806, 2012.

[19] Y. Jang, and M. M. Jovanovic, "A bridgeless PFC boost rectifier with optimized magnetic utilization," *IEEE Trans. Power Electron.*, Vol.24, No.1, pp. 85-93, Jan. 2009.

[20] X.D Huang, X.Y Wang, T. Nergaard, J.S Lai, X.Y Xu, and L. Zhu, "Parasitic ringing and design issues of digitally controlled high power interleaved boost converters," *IEEE Trans. Power Electron.*, Vol. 19, No. 5, pp. 1341-1352, Sep. 2004.

[21] Y. Hsieh, T. Hsueh, and H. Yen, "An interleaved boost converter with zero-voltage transition," *IEEE Trans. Power Electron.*, Vol. 24, No. 4, pp. 973-978, Apr. 2009.

[22] Y. L Chen, H. J. Chen, Y. M. Chen, and K. H. Liu, "A stepping on-time adjustment method for interleaved multichannel PFC converters," *IEEE Trans. Power Electron.*, Vol. 30, No. 3,pp. 1170-1176, Mar. 2015.

[23] W. F. Zhang, Y. F. Liu, and B. Wu, "A new duty cycle control strategy for power factor correction and FPGA implementation," *IEEE Trans. Power Electron.*, Vol. 21, No. 6, pp. 1745-1753, Nov. 2006.

[24] H. C. Chen, and J. Y. Liao, "Modified interleaved current sensorless control for three-level boost PFC converter with considering voltage imbalance and zero-crossing current distortion," *IEEE Trans. Ind. Electron.*, Vol.62, No.11, pp.6896-6904, Nov. 2015.

[25] K. Yao, X. B. Ruan, X. J. Mao, and Z. H. Ye, "Variable-duty-cycle control to achieve high input power factor for DCM boost PFC converter," *IEEE Trans. Ind. Electron.*, Vol. 58, No. 5, pp. 1856-1865, Apr. 2011.
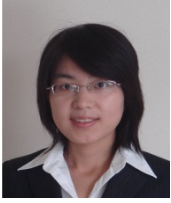
Miao-miao Cheng was born in China in 1982. She received her M.Sc. degree from Xi'an Jiaotong University, China, in 2006, and her Ph.D. degree from the Tokyo Institute of Technology (TIT) in 2009. She worked at TIT as a Post-doctoral Researcher for three years. Since 2012, she has been an Assistant Professor at Hunan University, China. Her research interests include motor control, reactive power compensation technologies, soft-switching power converters, and distributed power systems.

Zhiguo Liu was born in China in 1992. He received his B.E. degree from Anhui Jianzhu University, China, in 2014. He is now pursuing his M.Sc. degree at Hunan University, China. His research interests include soft-switching power converters and distributed power systems.

Yueyue Bao was born in China in 1991. He received his B.E. degree from Zhejiang University of Technology, China, in 2013. He is currently pursuing his M.Sc. degree at Hunan University, China. His research interests focus on the stability improvement of distributed systems.

Zhongjie Zhang was born in China in 1989. He received his B.E. degree from Hunan Institute of Technology, China, in 2012. From 2012 to 2013, he worked at Lens Technology Limited Corporation, Changsha. He is currently pursuing his M.Sc. degree at Hunan University, China. His research interests focus on high power density and high efficiency power converters.